Organic Electronics 11 (2010) 1103–1110

Contents lists available at ScienceDirect

Organic Electronics

journal homepage: www.elsevier.com/locate/orgel

Naphtho[2,3,*a*]pyrene as an efficient multifunctional organic semiconductor for organic solar cells, organic light-emitting diodes, and organic thin-film transistors

Jongchul Kwon [a,1], Jung-Pyo Hong [a,1], Woochul Lee [a], Seunguk Noh [b], Changhee Lee [b], Seonghoon Lee [a,*], Jong-In Hong [a,**]

[a] *Department of Chemistry, College of Natural Sciences, Seoul National University, Seoul 151-747, Republic of Korea*
[b] *School of Electrical Engineering and Computer Science, Inter-University Semiconductor Research Center, Seoul National University, Seoul 151-742, Republic of Korea*

ARTICLE INFO

Article history:
Received 7 January 2010
Received in revised form 26 March 2010
Accepted 29 March 2010
Available online 2 April 2010

Keywords:
Naphtho[2,3,*a*]pyrene
Multifunctional organic semiconductor
Organic solar cells
Organic light-emitting diodes
Organic thin-film transistors

ABSTRACT

We found that naphtho[2,3,*a*]pyrene (**NP**) can be commonly used as an effective tri-functional material for three representative kinds of devices in organic electronics. In order to prove the fact, we fabricated organic solar cells (OSCs), organic light-emitting diodes (OLEDs), and organic thin-film transistors (OTFTs) using **NP** as their active layer. First, an optimized 80 nm-thick **NP** based OSC device exhibited a good power conversion efficiency of 0.48% in OSCs. Second, OLEDs with 3% **NP** doping showed sky blue emission and a power efficiency of 3.4 lm W^{-1} and a current efficiency of 4.4 cd A^{-1}. OLEDs with 5% **NP** doping showed green emission and a power efficiency of 1.8 lm W^{-1} and a current efficiency of 3.9 cd A^{-1}. Third, OTFTs based on **NP** exhibited a field-effect mobility (μ_{FET}) of 0.12 $cm^2 V^{-1} s^{-1}$, a threshold voltage (V_{th}) of −10.8 V, and an on/off ratio of 6.8×10^6. These results indicated that **NP** can be efficiently used as a donor material in OSCs, a blue and green emitting material in OLEDs, and a charge transport channel in OTFTs.

1. Introduction

Since the first report on organic solar cells (OSCs) [1a], organic light-emitting diodes (OLEDs) [1b], and organic thin-film transistors (OTFTs) [1c], the development of organic electronics has attracted considerable attention owing to their advantages of low cost, easy device fabrication, and potential applications such as flexible displays, photovoltaic panels, radio-frequency identification tags (RFIDs), electronic sensors, and integrated electronic circuits. Several researchers have focused on improving the efficiency of the individual devices in optoelectronics using organic molecules [2–4].

Regarding the manufacturing process of organic electronic devices, one of the important issues is the low cost and simple device fabrication. For example, one important application of multifunctional organic materials can be found in the area of RFID manufactured using an all-in-line printing process [5]. The RFID manufacturing technology comprises rectifiers, antennas, powering devices, transistors, and displays, all integrated into a plastic foil or paper. Considering that fabrication of one kind of device would require a series of more than 10 patterning, material deposition and post-processing steps, that of RFID devices would include more than 50 discrete manufacturing steps. The cost for this RFID technology would be enormous. This problem can only be solved by introducing multifunctional materials that can be used in different devices in parallel. This should lead to much simpler electronic systems.

Generally, multifunctional materials need to be equipped with unique properties such as their light emit-

* Corresponding author. Tel.: +82 2 880 6682; fax: +82 2 889 1568.
** Corresponding author.
E-mail addresses: shnlee@snu.ac.kr (S. Lee), jihong@snu.ac.kr (J.-I. Hong).
[1] Both authors contributed equally to this work.

1566-1199/$ - see front matter © 2010 Elsevier B.V. All rights reserved.
doi:10.1016/j.orgel.2010.03.017

ting, light absorbing, and charge transporting ability in order to be able to perform multiple functions in OSCs, OLEDs, and OTFTs. Thus, it is rare to use the same organic materials as the active layer in individual devices based on different mechanisms. For these reasons, only a few dual functional or tri-functional organic materials have been reported in the literature [6,7]. For dual functional materials, rubrene [6a], triphenylamine–thiophene derivatives [6b], and triarylamine–carbazole based dendrimers [6c] have been investigated as both OLEDs emitting and OSCs donor material and tri-functional materials for the use in OSCs, OLEDs, and OTFTs using triphenylamine–oligothiophene conjugated molecules and fluorene–silole conjugated copolymers have been reported [7]. However, tri-functional materials based on triphenylamine–oligothiophene conjugated molecules showed a power conversion efficiency of 0.32% in OSCs, a poor green light emitting efficiency in OLEDs, and a field-effect mobility of 1.1×10^{-2} $cm^2 V^{-1} s^{-1}$ and on/off current ratio of 200 in OTFTs [7a]. Also, while a tri-functional material based on fluorene–silole conjugated copolymers showed a good power conversion efficiency of 2.01% in OSC devices, it showed a poor red emitting ability of external quantum efficiency of 0.17% in OLEDs, and poor field-effect mobility of 4.5×10^{-5} $cm^2 V^{-1} s^{-1}$ in OTFTs [7b]. The overall efficiency of these tri-functional materials is not high.

On the other hand, acene derivatives [8] have been extensively investigated as organic semiconductors for individual optoelectronic devices [9–11]. In particular, among the acene molecules, tetracene [12,17], pentacene [13,14,18], picene [15], anthanthrene [16], anthradithiophene [19a], and anthracene [19b], derivatives have been widely investigated as useful organic semiconductors for OSCs, OLEDs, and OTFTs [12–16,19]. However, tri-functional acene materials which can be used for emitting material in OLEDs, donor material in OSCs, and active material in OTFTs have not, to our knowledge, been reported so far in the literature.

Herein, we report that naphtho[2,3,*a*]pyrene (**NP**) (Fig. 1), a fused aromatic acene, can be utilized as an efficient multifunctional organic semiconductor material for optoelectronic devices to fabricate OSCs, OLEDs, and OTFTs devices by a vacuum deposition method. **NP** exhibited a maximum power conversion efficiency of 0.48% in OSCs which is considered a good efficiency among the acene molecules [19]. In addition, sky blue OLEDs at 3% **NP** doping exhibited a current efficiency of 4.4 cd A^{-1} and a power efficiency of 3.4 lm W^{-1} which are considered generally good EL efficiencies compared to that of sky blue acene based dopants such as chrysene [10] and anthanthrene derivatives [16a,b]. Also, 5% **NP** doping green OLEDs exhibited a power efficiency of 1.8 lm W^{-1} and a current efficiency of 3.9 cd A^{-1}. In particular, OTFTs using **NP** as an active layer exhibited a field-effect mobility (μ_{FET}) of 0.12 $cm^2 V^{-1} s^{-1}$, a threshold voltage (V_{th}) of −10.8 V, and an on/off current ratio of 6.8×10^6.

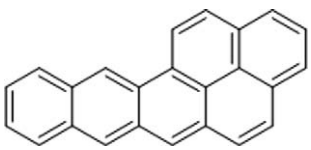

Fig. 1. Molecular structure of **NP**.

2. Experimental

2.1. Materials and instrument

The organic materials such as **NP**, C_{60}, CuPc, NPD, BPhen, and CBP were purchased from Aldrich, Lumtree, and Gracel. Poly(3,4-ethylenedioxythiophene):poly(styrenesulfonate) (PEDOT:PSS) was purchased from H.C. Stark. All the materials were purified by temperature gradient vacuum sublimation prior to use for devices. UV–Vis spectra were recorded on a Beckman DU 650 spectrophotometer. Fluorescence spectra were recorded on a Jasco FP-7500 spectrophotometer. Cyclic voltammetry (CV) was performed using a CH Instruments 660 Electrochemical Analyzer (CH Instruments, Inc., Texas). AFM experiments were performed using an asylum MFP-3D instrument in AC mode with Si_3N_4 cantilevers and XRD analyses were carried out with a Rigaku (λ = 1.5418 Å, 298 K) X-ray instrument. Decomposition temperatures (T_d) were obtained using a Q−5000−IR TGA instrument.

2.2. OSCs fabrication

A 30 nm-thickness of PEDOT:PSS was used as a hole injection layer (HIL). The thin film thickness of **NP** was prepared by an evaporation process from 10 to 100 nm. Then, a 30 nm-thickness of fullerene (C_{60}) as an acceptor was also evaporated. Next, a 8 nm-thickness layer of 4,7-diphenyl-1,10-phenanthroline (Bphen) as a exciton blocking layer (EBL) was evaporated. Finally, 100 nm-thickness of aluminum was evaporated onto the Bphen layer (Fig. S2). The current–voltage measurements of the devices were measured on a Keithley 237 instrument. The device performances were characterized under uniform illumination (AM 1.5G illumination intensity of 100 mW cm^{-2}) using a solar simulator (Newport, 91160A). The light intensity at each wavelength was calibrated using the standard Si solar cell as a reference.

2.3. OLEDs fabrication

A 10 nm-thickness of copper phthalocyanine (CuPc) was used as a hole injection layer (HIL) and a 30 nm-thickness of 4,4′-bis[*N*-(naphthyl-*N*-phenylamino)biphenyl (NPD) was used as a hole transport layer (HTL). A 30 nm-thickness of emitting layer (EML) was prepared by co-evaporating *N*,*N*′-dicarbazolyl-4,4′-biphenyl (CBP) as a host and 1, 3, 5 wt.% of **NP** as a fluorescent dopant. The fluorescent dopant concentration of **NP** was varied from 1 to 5 wt.%. Next, 30 nm-thickness layer of 4-biphenyloxolatoaluminium(III)bis(2-methyl-8-quinolinato)-4-phenylphenolate (Balq), as a hole blocking layer (HBL) and electron transporting layer (ETL) was evaporated. Then, LiF as an electron injection layer (EIL) was also evaporated. Finally, a 100 nm-thickness of aluminum was deposited on the LiF layer (Fig. S3). The emission properties were

determined using PR650 spectra scan spectracolorimeter as a source meter.

2.4. OTFTs fabrication

The transistors based on **NP** were fabricated with the top-contact geometry. We used a heavily doped Si wafer as the gate electrode and non-pretreated or octadecyltrichlorosilane (OTS)-pretreated SiO_2 layer (thickness, ca. 300 nm) as the gate dielectric. Prior to deposition, the **NP** starting material was purified by temperature gradient vacuum sublimation to improve the purity of the active layer. The **NP** films (ca. 500 Å) were then grown by vacuum sublimation, using a home-made apparatus, at a rate range of 0.4–0.8 Å s^{-1} under a working pressure of 2.0–2.5 $\times$ 10^{-6} torr. Gold source/drain electrodes were evaporated on top of the films through a shadow mask with a channel length (L) of 50 μm and a channel width (W) of 1000 μm (Fig. S6). Electrical characterization of the transistors was performed at room temperature in air by using a Keithley 4200-SCS semiconductor analyzer. The field-effect mobility (μ) was calculated in the saturation region (V_{DS} = −100 V) from the plot of the square-root of drain current vs. V_{GS} using the following equation: $I_{DS} = (W\text{-}C_i\mu(V_{GS} - V_T)^2)/2L$, where I_{DS} is the source-drain saturation current; C_i (1.1 $\times$ 10^{-8} F) is the capacitance of the SiO_2 insulator; W/L is the ratio of the width to the channel length; V_{GS} and V_T are the gate-source and threshold voltages, respectively.

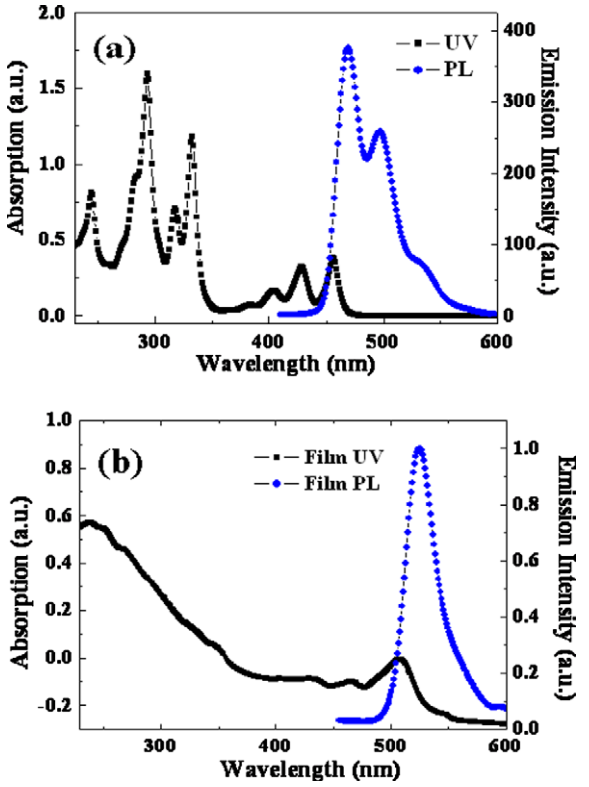

Fig. 2. UV and PL spectra of 0.02 mM **NP** in CH_2Cl_2 (a) and solid film (b).

3. Results and discussion

The UV spectra of **NP** show multiple absorption bands at 292, 332, 428, and 456 nm in CH_2Cl_2 and broad absorption bands at 269, 465, and 507 nm in solid film, respectively. The PL spectra of **NP** show sky blue emission at 468 and 497 nm in CH_2Cl_2 and green emission at 523 nm in solid film, respectively (Fig. 2). Both film UV and PL spectra of **NP** were significantly red-shifted in comparison with those in CH_2Cl_2, which is attributed to the flat structure of the **NP** molecule.

The photoluminescence quantum yield of **NP** was estimated to be 0.61 using anthracene as a standard [20]. Thermal gravimetric analysis (TGA) data reveal that **NP** has high thermal stability (T_d = 271 °C, Fig. S7).

In order to study the electrochemical properties of **NP**, we measured the cyclic voltammetry. **NP** shows a reversible oxidation process associated with stable cation radical generation. On the other hand, the reduction potential of **NP** was not observed in cyclic voltammetry. The half oxidation potential of **NP** was observed at $E_{1/2}$ = 0.50 V after ferrocene/ferrocenium correlation (Fig. S1). From these results, the HOMO energy value of **NP** (−5.30 eV) was calculated. The LUMO energy value of **NP** (−2.80 eV) was calculated from the cross-section wavelength between absorption and emission spectra (Table 1).

To investigate the efficient multifunctional properties of **NP**, we fabricated three representive types of organic electronic devices. First, we fabricated OSCs with the configuration of ITO/PEDOT:PSS (30 nm)/**NP** (x nm)/C_{60} (30 nm)/Bphen (8 nm)/Al (100 nm). The thickness of **NP** was varied from 10 to 100 nm.

Fig. 3 shows the current density vs. voltage (I–V) characteristics of heterojunction solar cells. All the OSCs show the solar cell behavior. Heterojunction solar cell using 10 nm-thick **NP** exhibited a significantly low power conversion efficiency (PCE) of 0.003% and short circuit current (I_{sc}) of 0.056 mA cm^{-2} due to the thin **NP** film, which cannot efficiently absorb the sunlight. On the other hand, an OSC device using 45 nm-thick **NP** exhibited the open circuit voltage (V_{oc}) of 0.37 V, short circuit current of 2.0 mA cm^{-2}, and power conversion efficiency of 0.35%, under simulated AM 1.5 solar irradiation at 100 mW cm^{-2}. In particular, when the thickness of **NP** was optimized at 80 nm, the OSC device exhibited a significantly increased power conversion efficiency of 0.48%, an open circuit voltage of 0.59 V, and a short circuit current of 1.9 mA cm^{-2}, under simulated AM 1.5 solar irradiation at 100 mW cm^{-2}. However, as the thickness of **NP** increased further to 100 nm, the device exhibited a significantly reduced short circuit current of 0.46 mA cm^{-2} and power conversion efficiency of 0.02% due to the thick **NP** film, in which excitons cannot be efficiently separated between hole and electron. We found that the performance of OSC devices using **NP** depends critically on the donor (**NP**) film thickness of the active layer. Typically, varying **NP** film thickness in the active layer resulted in changing the power conversion efficiency from 0.003% to 0.48%. Despite the narrow absorption range of **NP**, the maximum power conversion

Table 1
Photophysical and electrochemical data of **NP**.

	Absorption (λ_{nm}) [$\varepsilon \times 10^4$ M^{-1} cm^{-1}] [a]	Emission (λ_{nm}) [b]	Φ[c]	HOMO (eV)[d]	LUMO (eV)[e]
NP	243(3.90), 292(7.70), 332(5.90), 404 (0.80), 428(1.55), 456(1.90) (solution) 269, 349, 405, 433, 465, 507 (film)	468, 497 (solution) 523 (film)	0.61	5.30	2.80

[a,b] The absorption and emission spectra were measured in 0.02 mM in CH_2Cl_2 solution and quartz solid film.
[c] Photoluminescence quantum yield (Φ_{PL}) was determined by anthracene reference in ethanol solution.
[d] HOMO energy level was determined in CH_2Cl_2 solution (0.1 M $TBAPF_6$).
[e] LUMO energy level was calculated from the cross-section wavelength between absorption and emission spectra.

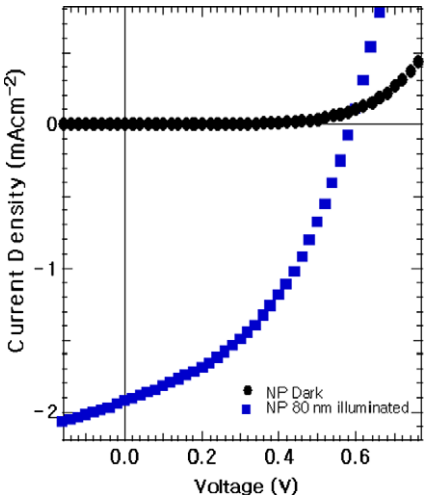

Fig. 3. *I–V* characteristics of ITO/PEDOT (30 nm)/**NP** (80 nm)/C_{60} (30 nm)/BPhen (8 nm)/Al (100 nm) device under simulated AM 1.5 solar irradiation at 100 mW cm^{-2}.

efficiency (0.48%) obtained in this study is considered high among the acene derivatives in OSCs (due to the good hole mobility of **NP**). This is the first report on **NP** based OSC donor materials. Our results indicate that among the acene derivatives, **NP** can be regarded as a good donor material for heterojunction solar cells. The overall device performance data based on **NP** and C_{60} are summarized in Table 2.

Second, OLED devices were fabricated using **NP** as a dopant molecule, with the configuration of ITO/CuPc (10 nm)/NPD (30 nm)/emitting layer (EML 30 nm)/Balq (30 nm)/LiF (1 nm)/Al (100 nm). Emitting layers of 30 nm-thickness were prepared by co-evaporating CBP as

Table 2
OSC data based on various film thickness of **NP** and C_{60} under simulated AM 1.5 solar irradiation at 100 mW cm^{-2}.

Thickness of **NP** (nm)	V_{OC} (V)[a]	I_{SC} (mA cm^{-2})[b]	FF (%)[c]	PCE (%)[d]
10	0.54	0.056	10	0.003
45	0.37	2.0	46	0.35
80	0.59	1.9	42	0.48
100	0.38	0.46	11	0.02

[a] Open circuit voltage.
[b] Short circuit current.
[c] Fill factor.
[d] Power conversion efficiency.

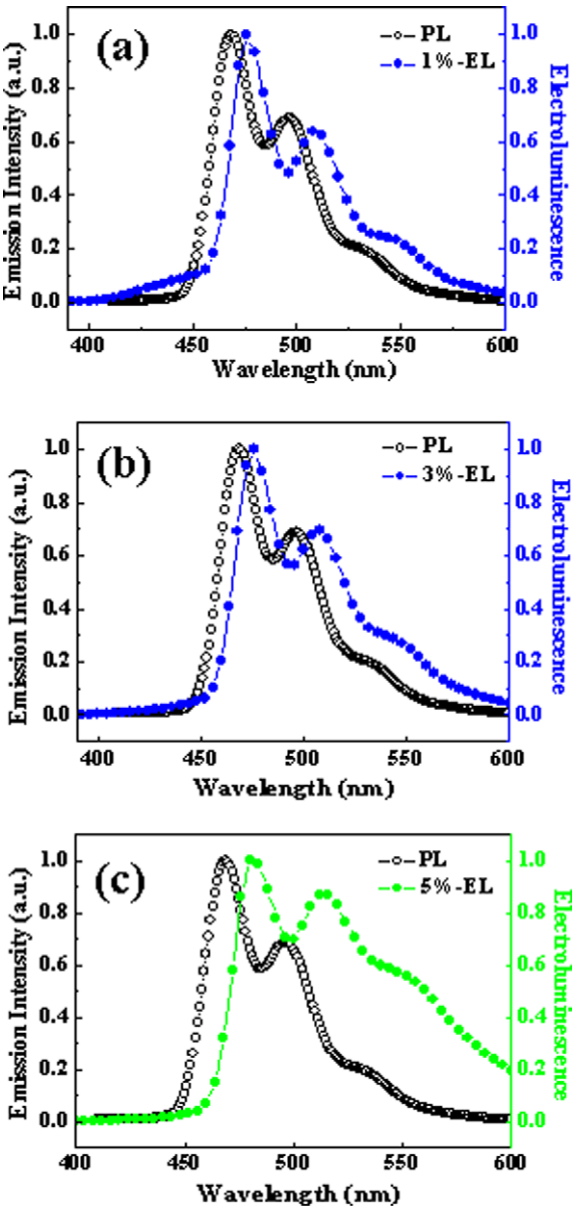

Fig. 4. EL spectra according to different **NP** doping ratios (a) 1%, (b) 3%, and (c) 5% in OLEDs with configuration of ITO/CuPc (10 nm)/NPD (30 nm)/EML (30 nm)/Balq (30 nm)/LiF (1 nm)/Al (100 nm).

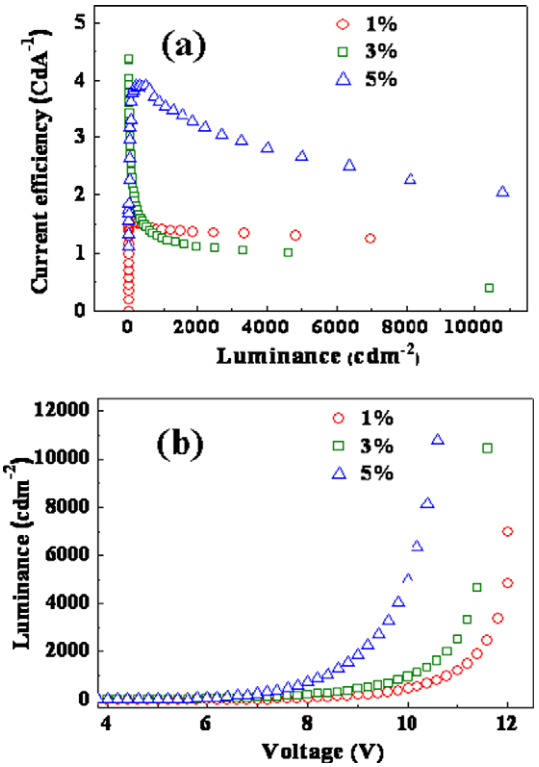

Fig. 5. Characteristics of ITO/CuPc (10 nm)/NPD (30 nm)/EML (30 nm)/Balq (30 nm)/LiF (1 nm)/Al (100 nm) devices. (a) Luminance (cd m^{-2}) vs. current efficiency (cd A^{-1}). (b) voltage (V) vs. luminance (cd m^{-2}).

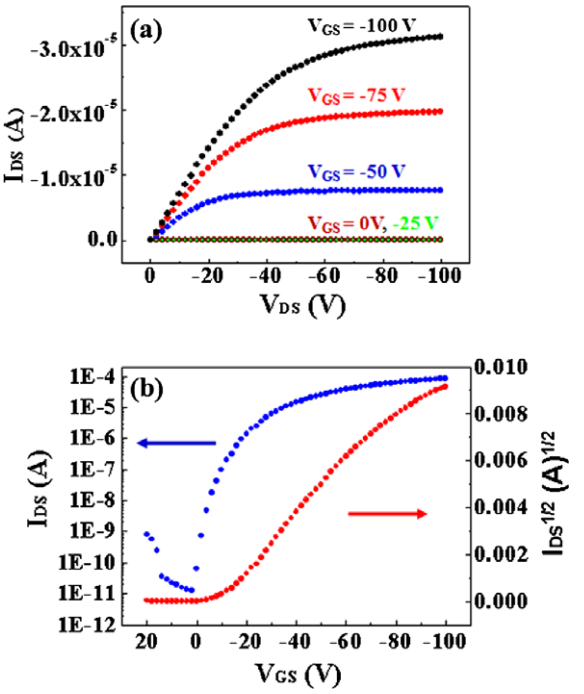

Fig. 6. The output (a) and transfer characteristics (b) of the OTFTs using **NP** deposited at T_{sub} = 75 °C on OTS-treated SiO_2.

Table 4
OTFT data.

T_{sub} (°C)	μ_{FET} (cm^2 V^{-1} s^{-1})[a]	V_{th} (V)[b]	I_{on}/I_{off}[c]
Bare SiO_2			
RT	0.02	−21.3	2.5×10^5
75	0.01	−17.8	4.2×10^5
110	No FET	–	–
OTS-SiO_2			
RT	0.05	−18.4	2.0×10^6
75	0.12	−10.8	6.8×10^6
110	0.005	−19.4	3.1×10^5

[a] Field-effect mobility.
[b] Threshold voltage.
[c] On–off ratio.

a host and *x* wt.% **NP** as a fluorescent dopant. Fig. 4 shows the photoluminescence (PL) in CH_2Cl_2 and electroluminescence (EL) spectra with different doping ratios of **NP**. The PL spectra of **NP** in CH_2Cl_2 show the sky blue emission centered at 468 and 497 nm. At 1% and 3% **NP** doping, the EL spectra show the similar sky blue emission compared to that of PL emission (Fig. 4).

The similar pattern of the PL and EL spectra of 1% and 3% **NP** doped device suggests that EL spectra should be attributed to an emission from a singlet excited state of **NP** in the emitting layer. On the other hand, the 5% **NP** doped device shows green emission centered at about 479, 514, and 550 nm (Fig. 4). This is most likely due to the formation of an excimer resulting from the aggregation of **NP** dopant molecules in the emitting layer. This could be due to the planar molecular structure of **NP**, which cannot prevent aggregation in the emitting layer. We were able to change the emission color from sky blue to green by varying the

Table 3
OLED data.

NP (%)[a]	Max η_p (lm W^{-1})[b]	Max η_c (cd A^{-1})[c]	Max η_{ext} (%)[d]	Max η_l (cd m^{-2})[e]	EL (λ_{nm})[f]	CIE
1	0.7	1.7	0.7	6988 at 12.0 V	476, 509	(0.16, 0.36)
3	3.4	4.4	1.8	10430 at 11.6 V	476, 512	(0.17, 0.39)
5	1.8	3.9	1.4	10780 at 10.6 V	479,514, 550	(0.31, 0.52)

[a] **NP** doping ratio. ITO/CuPc (10 nm)/NPD (30 nm)/EML (30 nm) **NP** *x* wt.% doping/Balq (30 nm)/LiF (1 nm)/Al (100 nm).
[b] Power efficiency.
[c] Current efficiency.
[d] External quantum efficiency.
[e] Luminance.
[f] The EL spectra were obtained from OLEDs.

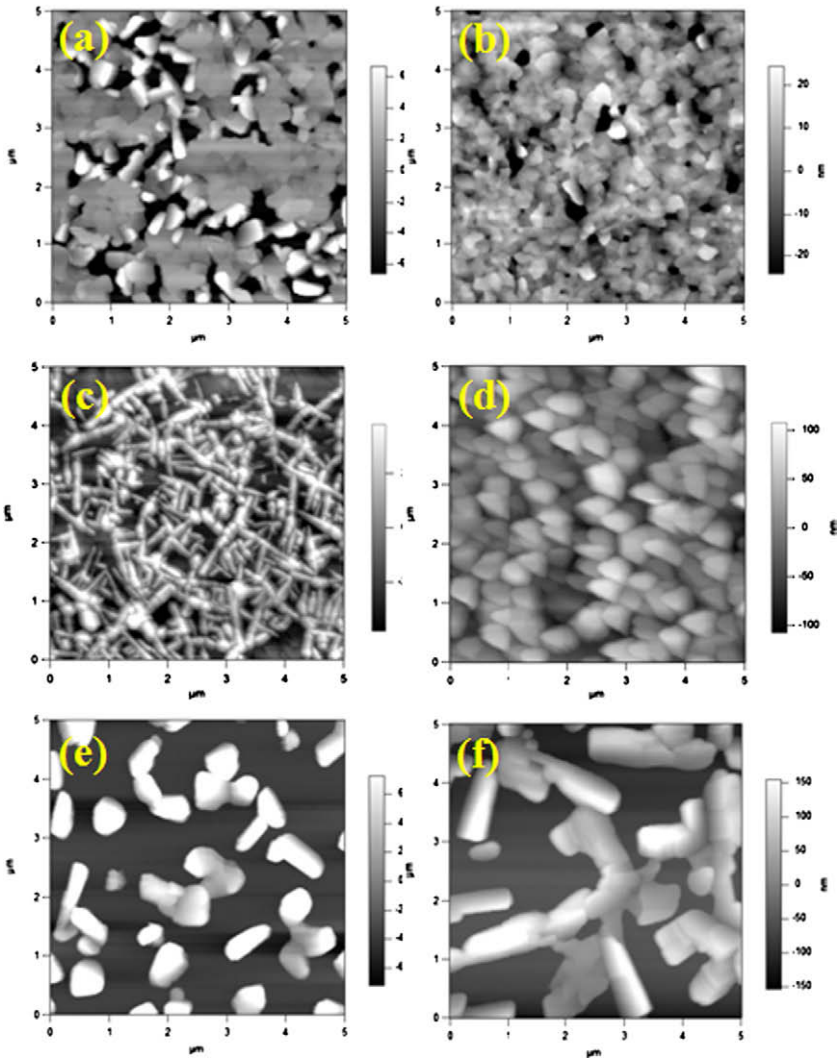

Fig. 7. 5 × 5 μm AFM topography images of 50 nm **NP** thin films (measured by the quartz crystal microbalance) deposited on SiO_2 (left column) and OTS/SiO_2 (right column) at various substrate temperatures: (a, b) RT; (c, d) 75 °C; (e, f) 110 °C.

NP doping ratio. This result indicates that the EL emission depends on the **NP** doping ratio in the emitting layer.

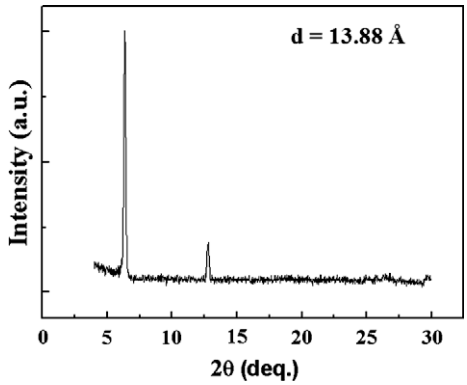

Fig. 8. X-ray diffraction (XRD) pattern of the thin films of **NP** grown on SiO_2 at RT.

Fig. 5 shows the sky blue and green emitting EL device data. The sky blue OLED device at 1% **NP** doping shows a power efficiency of 0.7 lm W^{-1} and current efficiency of 1.7 cd A^{-1}. In particular, the OLED device at 3% **NP** doping shows the maximum power efficiency of 3.4 lm W^{-1} and current efficiency of 4.4 cd A^{-1}, and a Commission Internationale de l'Eclairage (CIE) coordinates of (0.17, 0.39). At 3% **NP** doping, the maximum power efficiency and current efficiency of the EL device are considered generally good. Therefore, the efficiencies of OLEDs using **NP** are higher than those of devices using other acene materials such as chrysene [10] and anthanthrene derivatives [16a,b].

Furthermore, at 5% **NP** doping, the green OLED device shows a power efficiency of 1.8 lm W^{-1} and current efficiency of 3.9 cd A^{-1}, and a CIE coordinates of (0.31, 0.52). As a result, the EL at 5% **NP** doping showed green emission with generally good luminous power efficiency and current efficiency in OLED devices. Also, the turn-on voltage is reduced as the doping concentration of **NP** increases. It

is presumably because **NP** can be used as efficient carrier transport channel at high doping concentration of **NP** (Fig. 5b) [16c]. All EL device data are summarized in Table 3. As a result, **NP** can be used as sky blue dopant material as well as green dopant material in fluorescent OLEDs. Although the operation mechanisms of OLEDs and OSCs are different, **NP** shows good efficiencies for both OLEDs and OSCs due to the good photoluminescence quantum yield and hole mobility.

Third, the possibility of **NP** being used for charge transport channels in OTFTs was investigated by the fabrication of OTFTs using top-contact geometry (Fig. S6).

Fig. 6 shows the output and transfer characteristics of top-contact OTFTs using **NP** deposited at a substrate temperature (T_{sub}) of 75 °C on OTS-treated SiO_2. From the electrical transfer characteristics, we obtained parameters such as the field-effect mobility, on/off current ratio, and threshold voltage for the devices. The OTFTs based on **NP** showed a field-effect mobility of 0.12 $cm^2 V^{-1} s^{-1}$, threshold voltage of −10.8 V, and on/off current ratio of 6.8×10^6 under ambient conditions. The electrical properties of **NP** based OTFT devices fabricated under various conditions are summarized in Table 4. To investigate the cause of the different OTFTs performance under various conditions, we studied the film morphology of thin **NP** active layers using atomic force microscopy (AFM). Fig. 7 shows AFM images of **NP** active layers deposited on SiO_2 (left column) and OTS/SiO_2 (right column) at RT, 75 °C, and 110 °C. The connectivity of **NP** grains deposited on a SiO_2 substrate at RT has poor, low field-effect mobility. However, **NP** films deposited on an OTS/SiO_2 substrate at RT show improved film connectivity and field-effect mobility. In particular, densely packed grains on an OTS/SiO_2 substrate at 75 °C were observed and showed the best field-effect mobility among **NP** based devices under various conditions, due to improved interconnectivity in the channels of the **NP** films. Also, at 110 °C, we observed that sub-micron-sized **NP** grains deposited on SiO_2 were disconnected, and as a result, showed no electrical properties. However, the films deposited on OTS/SiO_2 were connected, and as a result, showed electrical properties.

When the morphological characteristics of thin-film **NP** were investigated by X-ray diffraction (XRD), the patterns displayed 2nd order diffraction peaks and the intense XRD peaks in low angle side indicated a highly ordered lamellar structure within **NP** with a period of 13.88 Å (Fig. 8).

4. Conclusion

We found that **NP** can be commonly used as an effective tri-functional material for three representative kinds of devices in organic electronics. In order to prove the fact, we fabricated the OSCs, OLEDs, and OTFTs using **NP** molecules as active layers. First, an optimized 80 nm-thick **NP** based OSC device exhibited a good power conversion efficiency of 0.48%. Second, an OLED device with 3% **NP** doping showed sky blue emission and a power efficiency of 3.4 lm W^{-1} and a current efficiency of 4.4 cd A^{-1}, and a CIE coordinates of (0.17, 0.39). OLEDs with 5% **NP** doping showed green emission and a power efficiency of 1.8 lm W^{-1} and a current efficiency of 3.9 cd A^{-1}. Third, OTFTs based on **NP** exhibited a field-effect mobility of 0.12 $cm^2 V^{-1} s^{-1}$, a threshold voltage of −10.8 V, and an on/off ratio of 6.8×10^6. Consequently, **NP** turned out to be a promising organic semiconductor material which can be used as an efficient blue or green light emitting material, and efficient solar cell donor, and an organic semiconductor for OTFTs. Further studies on modified **NP** based organic semiconductors for optoelectronic devices are in progress.

Acknowledgements

This work was supported by Basic Science Research Program through the National Research Foundation of Korea (NRF) grant funded from the Ministry of Education, Science and Technology (MEST) of Korea for the Center for Next Generation Dye-sensitized Solar Cells (No. 2010-0001842), the National Research Foundation of Korea Grant funded by the Korean Government (MEST) (NRF-C1AAA001-2009-0093282), KOSEF through CNNC, and the Seoul R&BD Program (10543). We also acknowledge the BK21 program and Nanosystems Institute National Core Research Center for student financial support.

Appendix A. Supplementary material

Supplementary data associated with this article can be found, in the online version, at doi:10.1016/j.orgel.2010.03.017.

References

[1] (a) C.W. Tang, Appl. Phys. Lett. 48 (1986) 183;
(b) C.W. Tang, S.A. VanSlyke, Appl. Phys. Lett. 51 (1987) 913;
(c) A. Tsumura, H. Koezuka, T. Ando, Appl. Phys. Lett. 49 (1986) 1210.
[2] (a) H. Meng, F. Sun, M.B. Goldfinger, G.D. Jaycox, Z. Li, W.J. Marshall, G.S. Blackman, J. Am. Chem. Soc. 127 (2005) 2406;
N.M. Kronenberg, M. Deppisch, F. Würthner, H.W.A. Lademann, K. Deing, K. Meerholz, Chem. Commun. (2008) 6489.
[3] (a) K.L. Mutolo, E.I. Mayo, B.P. Rand, S.R. Forrest, M.E. Thompson, J. Am. Chem. Soc. 128 (2006) 8108;
(b) F. Silvestri, M.D. Irwin, L. Beverina, A. Facchetti, G.A. Pagani, T.J. Marks, J. Am. Chem. Soc. 130 (2008) 17640;
(c) C. He, Q. He, Y. Yi, G. Wu, F. Bai, Z. Shuai, Y. Li, J. Mater. Chem. 18 (2008) 4085.
[4] (a) M.-C. Um, J. Kwak, J.-P. Hong, J. Kang, D.Y. Yoon, S.H. Lee, C. Lee, J.-I. Hong, J. Mater. Chem. 18 (2008) 4698;
(b) M.-C. Um, J. Jang, J.-P. Hong, J. Kang, D.Y. Yoon, S.H. Lee, J.-J. Kim, J.-I. Hong, New J. Chem. 32 (2008) 2006;
(c) J.-P. Hong, A.-Y. Park, S. Lee, J. Kang, N. Shin, D.Y. Yoon, Appl. Phys. Lett. 92 (2008) 143311;
(d) J.A. Letizia, A. Facchetti, C.L. Stern, M.A. Ratner, T.J. Marks, J. Am. Chem. Soc. 127 (2005) 13476;
(e) J.-P. Hong, S. Lee, Angew. Chem., Int. Ed. 48 (2009) 3096;
(f) A. Facchetti, M. Mushrush, M.-H. Yoon, G.R. Hutchison, M.A. Ratner, T.J. Marks, J. Am. Chem. Soc. 126 (2004) 13859;
(g) M. Mushrush, A. Facchetti, M. Lefenfeld, H.E. Katz, T.J. Marks, J. Am. Chem. Soc. 125 (2003) 9414.
[5] M. Berggren, D. Nilsson, N.D. Robinson, Nature Mater. 6 (2007) 3.
[6] (a) A.K. Pandey, J.-M. Nunzi, Adv. Mater. 19 (2007) 3613;
(b) A. Cravino, P. Leriche, O. Alévêque, S. Roquet, J. Roncali, Adv. Mater. 18 (2006) 3033;
(c) J. Lu, P.F. Xia, P.K. Lo, Y. Tao, M.S. Wong, Chem. Mater. 18 (2006) 6194.
[7] (a) A. Cravino, S. Roquet, O. Alévêque, P. Leriche, P. Frère, J. Roncali, Chem. Mater. 18 (2006) 2584;

(b) F. Wang, J. Luo, K. Yang, J. Chen, F. Huang, Y. Cao, Macromolecules 38 (2005) 2253.
[8] (a) J.E. Anthony, Chem. Rev. 106 (2006) 5028;
(b) J.E. Anthony, Angew. Chem., Int. Ed. 47 (2008) 452;
(c) S. Subramanian, S.K. Park, S.R. Parkin, V. Podzorov, T.N. Jackson, J.E. Anthony, J. Am. Chem. Soc. 130 (2008) 2706;
(d) K.C. Dickey, J.E. Anthony, Y.-L. Loo, Adv. Mater. 18 (2006) 1721;
(e) M.-C. Um, J. Jang, J. Kang, J.-P. Hong, D.Y. Yoon, S.H. Lee, J.-J. Kim, J.-I. Hong, J. Mater. Chem. 18 (2008) 2234;
(f) J.-P. Hong, M.-C. Um, S.-R. Nam, J.-I. Hong, S. Lee, Chem. Commun. (2009) 310.
[9] R.J. Tseng, R. Chan, V.C. Tung, Y. Yang, Adv. Mater. 20 (2008) 435.
[10] A.S. Ionkin, W.J. Marshall, B.M. Fish, L.M. Bryman, Y. Wang, Chem. Commun. (2008) 2319.
[11] M.M. Payne, S.R. Parkin, J.E. Anthony, C.-C. Kuo, T.N. Jackson, J. Am. Chem. Soc. 127 (2005) 4986.
[12] S.A. Odom, S.R. Parkin, J.E. Anthony, Org. Lett. 5 (2003) 4245.
[13] M.A. Wolak, J. Delcamp, C.A. Landis, P.A. Lane, J. Anthony, Z. Kafafi, Adv. Funct. Mater. 16 (2006) 1943.
[14] C.D. Sheraw, T.N. Jackson, D.L. Eaton, J.E. Anthony, Adv. Mater. 15 (2003) 2009.
[15] H. Okamoto, N. Kawasaki, Y. Kaji, Y. Kubozono, A. Fujiwara, M. Yamaji, J. Am. Chem. Soc. 130 (2008) 10470.
[16] (a) B.K. Shah, D.C. Neckers, J. Shi, E.W. Forsythe, D. Morton, J. Phys. Chem. A 109 (2005) 7677;
(b) B.K. Shah, D.C. Neckers, J. Shi, E.W. Forsythe, D. Morton, Chem. Mater. 18 (2006) 603;
(c) T. Zheng, W.C.H. Choy, Adv. Funct. Mater. 20 (2010) 651–652.
[17] C.-W. Chu, Y. Shao, V. Shrotriya, Y. Yang, App. Phys. Lett. 86 (2005) 243506.
[18] S. Yoo, B. Domercq, B. Kippelen, App. Phys. Lett. 85 (2004) 5427.
[19] (a) M.T. Lloyd, A.C. Mayer, S. Subramanian, D.A. Mourey, D.J. Herman, A.V. Bapat, J.E. Anthony, G.G. Malliaras, J. Am. Chem. Soc. 129 (2007) 9144;
(b) L. Valentini, D. Bagnis, A. Marrocchi, M. Seri, A. Taticchi, J.M. Kenny, Chem. Mater. 20 (2008) 32.
[20] W.R. Dawson, M.W. Windsor, J. Phys. Chem. 72 (1968) 3255.